Journal of Biomolecular NMR (2019) 73:699–712
https://doi.org/10.1007/s10858-019-00282-0

ARTICLE

Paramagnetic-iterative relaxation matrix approach: extracting PRE-restraints from NOESY spectra for 3D structure elucidation of biomolecules

E. C. Cetiner[1] · H. R. A. Jonker[1] · C. Helmling[1] · D. B. Gophane[2] · C. Grünewald[1] · S. Th. Sigurdsson[2] · H. Schwalbe[1]

Received: 24 April 2019 / Accepted: 27 September 2019 / Published online: 12 October 2019

Abstract
Paramagnetic relaxation enhancement (PRE) can be used to determine long-range distance restraints in biomolecules. The PREs are typically determined by analysis of intensity differences in HSQC experiments of paramagnetic and diamagnetic spin labels. However, this approach requires both isotope- and spin-labelling. Herein, we report a novel method to evaluate NOESY intensities in the presence of a paramagnetic moiety to determine PRE restraints. The advantage of our approach over HSQC-based approaches is the increased number of available signals without the need for isotope labelling. NOESY intensities affected by a paramagnetic center were evaluated during a structure calculation within the paramagnetic iterative relaxation matrix approach (P-IRMA). We applied P-IRMA to a 14-mer RNA with a known NMR solution structure, which allowed us to assess the quality of the PRE restraints. To this end, three different spin labels have been attached at different positions of the 14-mer to test the influence of flexibility on the structure calculation. Structural disturbances introduced by the spin label have been evaluated by chemical shift analysis. Furthermore, the impact of P-IRMA on the quality of the structure bundles were tested by intentionally leaving out available diamagnetic restraints. Our analyses show that P-IRMA is a powerful tool to refine RNA structures for systems that are insufficiently described by using only diamagnetic restraints.

Keywords RNA · IRMA · PRE · NMR · Paramagnetic · Spin label · NOESY

Introduction

Nuclear magnetic resonance spectroscopy (NMR) is a key technique to determine the three-dimensional structure of proteins and oligonucleotides and their complexes. In particular, NMR contributed to the determination of about 40% of RNA structures known so far. However, only RNA structures up to approx. 60 nucleotides in size have been determined, in part because the nuclear Overhauser effect (NOE) only provides short-range distance constraints. A particularly powerful approach to overcome this size limitation is the incorporation of a paramagnetic spin label. Paramagnetic effects can induce residual dipolar couplings (RDCs), pseudo contact shifts (PCS) and paramagnetic relaxation enhancements (PREs) and can be exploited to obtain additional structural information that can be incorporated into the NMR structure calculation as orientational and long-range distance restraints.

The PRE effect can be evaluated from well resolved peaks. To acquire the necessary peak resolution in biomolecules the PRE effect is commonly determined by quantifying crosspeak intensity reduction in 2D HSQC (heteronuclear single quantum coherence) NMR experiments and applications range from proteins (Battiste and Wagner 2000; Dedmon et al. 2005; Volkov et al. 2006) to protein–nucleic acid complexes (Mackereth et al. 2011; Ramos and Varani 1998) and nucleic acids (Helmling et al. 2014; Wunderlich et al. 2013). In addition to incorporation of a spin label, the HSQC approach requires ^{13}C

Electronic supplementary material The online version of this article (https://doi.org/10.1007/s10858-019-00282-0) contains supplementary material, which is available to authorized users.

✉ H. Schwalbe
Schwalbe@nmr.uni-frankfurt.de

[1] Institut für Organische Chemie und Chemische Biologie, Zentrum für Biomolekulare Magnetische Resonanz, Goethe Universität Frankfurt am Main, Max-von-Laue Straße 7, 60438 Frankfurt am Main, Germany

[2] Department of Chemistry Science Institute, University of Iceland, Dunhaga 3, 107 Reykjavik, Iceland

and ^{15}N isotope labelling of the biomolecule. For proteins, site-specific spin and simultaneous isotope labelling is a well-established procedure. For isotope-labelled RNAs, site-specific spin labelling can be easily realised in terminal position (Macosko et al. 1999). Alternatively, chemical synthesis of spin labelled nucleic acids or their precursors enables flexible spin label positioning; yet, it is accompanied by a size limitation of the RNA and high cost originating from isotope labelling. Thus, the latter is generally omitted, rendering the RNAs obtained unsuitable for HSQC experiments. Larger nucleic acids are accessible by ligation (Büttner et al. 2013) or non-covalent spin labelling (Helmling et al. 2014; Schnorr et al. 2017). However, these approaches usually lead to only partially isotope labelled constructs, which decreases the number of already limited restraints for structure calculation. An important aspect, which needs to be considered for ligation of spin labelled nucleotides is the reducing agents (e.g. Dithiothreitol DTT) necessary for most ligases. So either a DTT independent ligase must be deployed (Büttner et al. 2013) or the spin label must be protected during ligation (Seven et al. 2014).

The incompatibility of simultaneous spin labelling and isotope labelling illustrates the necessity of an alternative approach to evaluate the PRE effect in oligonucleotides of interest. Already in a small 14-mer tetraloop RNA 81% of all non-exchanging signals overlap (see SI for examplator spectrum, Fürtig et al. 2004). This overlap increases significantly for increasingly large RNAs. Quantity and distribution of PRE distance restraints are essential to gain structural insight on a biomolecule. It is therefore unfeasible to rely on non-overlapping signals from one dimensional proton spectra. In an effort to increase the accessibility of PRE distance restraints of non-isotope labelled samples, we developed an NOESY-based approach.

The distance dependence of the PRE effect on NOE crosspeak intensities has been evaluated qualitatively as assignment strategy (Unger et al. 1985) for naturally paramagnetic species. Recently, this assignment strategy has been revisited for freely diffusing paramagnetic species (Kellner et al. 2009). A more quantitative analysis of the PRE effect on NOE intensities has been conducted by Beswick et al. (1998). By analysis of the NH-CαH crosspeak linewidth at half-height, the authors determined the orientation of a protein fragment in dodecylphosphocholine micelles. However, their analysis comprised a comparison of relative proximity to the spin label instead of the determination of specific distance restraints.

Herein, we report a new NOESY-based, paramagnetic iterative relaxation matrix approach (P-IRMA) for the determination of three-dimensional biomolecular structures, which does not require costly isotope labelling. Quantitative PRE analysis of 2D ^{1}H–^{1}H-NOESY crosspeak intensities provides an easy access to long-range distance information and appears generalizable for larger RNA constructs.

Theory

The NOE between spins I and S is influenced by two processes: cross-relaxation and auto-relaxation, described by the cross relaxation rate σ_{IS} (1) and the auto-relaxation rate ρ_{IS}, respectively (Solomon 1955).

$$\sigma_{IS} = \frac{1}{20}\left(\frac{\mu_0\gamma_I\gamma_S\hbar}{4\pi r_{IS}^3}\right)^2\left(6J\left(\omega_I+\omega_S\right)-J\left(\omega_I-\omega_S\right)\right) \tag{1}$$

$$\rho_{IS} = \frac{1}{10}\left(\frac{\mu_0\gamma_I\gamma_S\hbar}{4\pi r_{IS}^3}\right)^2\left(J\left(\omega_I-\omega_S\right)+3J\left(\omega_I\right)+6J\left(\omega_I+\omega_S\right)\right) \tag{2}$$

where μ_0 is the magnetic permeability of free space, γ_I and γ_S are the gyromagnetic ratios of the involved spins I and S, $\hbar$ the reduced Planck constant, r_{IS} the distance between the involved spins, ω_n the angular frequency of the involved spin and J the spectral density function (3).

$$J(\omega) = \frac{2\tau_c}{1+\omega^2\tau_c^2} \tag{3}$$

The spectral density function is dependent on the total correlation time of the molecule, which is the reason for the molecular size dependence of the NOE. (1) and (2) can be used to describe a two spin system, but can also be adapted for a multiple spin system. For this purpose, a relaxation matrix can be constructed by describing every cross relaxation event according to (1) and the auto-relaxation according to (4).

$$\rho_i = \sum_{j\neq i}\rho_{ij} \tag{4}$$

This can be depicted in a relaxation matrix as seen in formula (5).

$$\underline{R} = \begin{bmatrix} \rho_1 & \sigma_{12} & \cdots & \sigma_{1n} \\ \sigma_{21} & \rho_2 & \cdots & \sigma_{2n} \\ \vdots & \vdots & \ddots & \vdots \\ \sigma_{n1} & \sigma_{n2} & \cdots & \rho_n \end{bmatrix} \tag{5}$$

PRE effects can be included in this model by addition of the paramagnetic relaxation rate Γ_I to the auto relaxation rate (6).

$$\rho_{i,para} = \Gamma_I + \sum_{j\neq i}\rho_{ij} \tag{6}$$

Assuming that the angular momentum of the electron is far greater than the angular momentum of the proton ($\omega_S \gg \omega_I$)

one can derive the following approximation (7) from formula (2):

$$\Gamma_1 = \frac{1}{10}\left(\frac{\mu_0\gamma_I\gamma_S\hbar}{4\pi r_{IS}^3}\right)^2\left(3J(\omega_I)+7J(\omega_S)\right) \tag{7}$$

The dependence of the NOE on the relaxation matrix is given by (8),

$$\underline{A} = e^{\underline{R}\tau_m}A(0) \tag{8}$$

with the mixing time τ_m, the intensity matrix $\underline{A}$ and the intensities at $t=0$, $A(0)$. With these formulae one can calculate the theoretical NOE intensities from a model structure.

Spin label flexibility

If the spin label is flexible the formulae must be augmented to cover the internal motion of the unpaired electron. Two effects must be considered for a flexible spin label. Firstly, multiple possible electron positions and, secondly, the effect of the correlation time of the internal movement on the relaxation rate must be taken into account. The model free approach by Lipari and Szabo (1982) covers both aspects.

The regular spectral density function is substituted by the model free spectral density function (9)

$$J_{MF} = \frac{S^2\tau_c}{1+(\tau_c\omega)^2} + \frac{(1-S^2)\tau_t}{1+(\tau_t\omega)^2} \tag{9}$$

with the order parameter S^2 and the total correlation time defined by (10)

$$\frac{1}{\tau_t} = \frac{1}{\tau_r} + \frac{1}{\tau_i} + \frac{1}{\tau_e} \tag{10}$$

with τ_i the correlation time of the internal movement. The order parameter is given by the following general expression (11)

$$S^2 = \overline{r_{IS}^{-6}}^{-1}\sum_{m=-2}^{2}\left|\frac{\overline{Y_2^m(\Omega)}}{r_{IS}^3}\right| \tag{11}$$

with r_{IS} the distance between the spins I and S and $Y_2^m(\Omega)$ the second order spherical harmonic of the Euler angles Ω. For the incorporation of the model free approach in the paramagnetic relaxation enhancement, the order parameter must be determined for every proton electron pair.

Under the assumption that there are N possible electron positions through which the electron jumps (different rotamers), the order parameter can be calculated by (12) (Brueschweiler et al. 1992)

$$S^2 = \left[\sum_{i=1}^{N} p_i r_i^{-6}\right]^{-1}\sum_{i,j=1}^{N} p_i p_j \frac{P_2(\cos\chi_{ij})}{r_i^3 r_j^3} \tag{12}$$

with p_i and p_j being the probability for the rotamer i and j,r_i and r_j the vector length between the electron i or j and the proton, χ_{ij} the angle between the vectors i and j and P_2 the second order polynomial given by (13).

$$P_2(x) = \frac{1}{2}\left(3x^2-1\right) \tag{13}$$

Materials and methods

Samples and NMR spectroscopy

The reference system for the approach used in this work is a 14-mer tetraloop RNA, whose NMR chemical shift values are fully assigned and an NMR-structure is available.(Fürtig et al. 2004; Nozinovic et al. 2010) To evaluate the influence of spin label flexibility, three different spin labels were selected (see Fig. 1).

Spin-label TPA (2,2,5,5-Tetramethylpyrrolin-1-yloxyl-3-acetylene) was synthesized according to literature (Azarkh et al. 2013). Oligonucleotide synthesis for 5TPA U7 was performed on a rebuilt ABI 392 synthesizer (Applied Biosystems) using Dharmacon´s 5′-O-Silylether Chemistry omitting acid conditions while 5′-deprotection and using peroxide oxidation. Both conditions are needed to not harm the spin label in the course of solid-phase

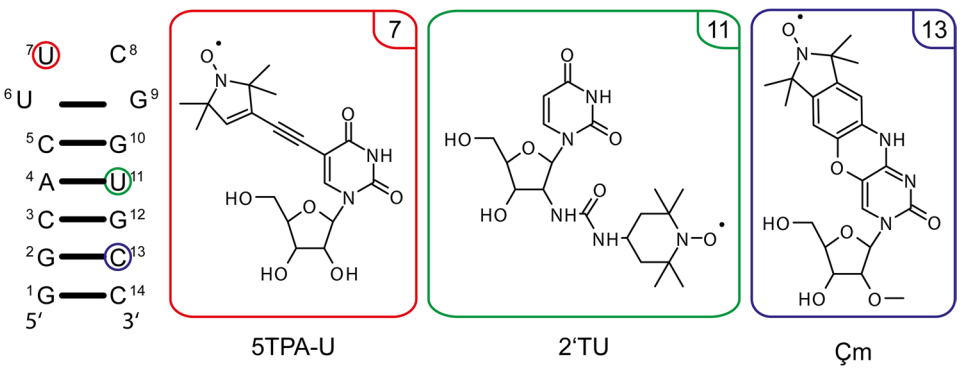

Fig. 1 14-mer RNA tetraloop with the spin-labels and spin-labelling positions used (marked in red, green and blue, respectively)

synthesis. Oligonucleotide synthesis and coupling TPA to 5-Iodouracil derivative by site-specific Sonogashira on solid support was performed applying reported protocols (Grünewald et al. 2008; Schiemann et al. 2007). The Çm13-14-mer was prepared as described in (Höbartner et al. 2012). A 2′-amino modified oligonucleotide was ordered at Dharmacon and spin-labelled according to the procedure reported by Edwards and Sigurdsson (Edwards and Sigurdsson 2007). All sample were purified with HPLC using a *Kromasil RP18*-coloumn with 0.1 M TEAAc (pH 6.5) and acetonitrile with a gradient of 0–100% in 50 min at a flowrate of 1 ml per minute. The HPLC purified samples were repeatedly lyophilised to remove volatile HPLC buffer components, reconstituted in water, precipitated in $LiClO_4$-acetone solution, reconstituted in phosphate buffer (50 mM KH_2PO_4/K_2HPO_4, pH 6.2) and transferred into D_2O via lyophilisation. The subsequent NOESY spectra were recorded on Bruker AV II 600 MHz (5TPA-U7 and Çm13) and Bruker AV I 700 MHz (2′TU11) spectrometers with the mixing times ranging from 100 to 750 ms in a scanwise interleaved manner, at a temperature of 298 K. To measure diamagnetic reference spectra, the samples were treated with 4 equivalents of ascorbic acid and all the NMR experiments were repeated after an 1 day incubation time.

P-IRMA

For evaluation of the structure-dependent and spin diffusion-corrected PRE restraints, we developed a procedure similar to the iterative relaxation matrix approach (IRMA, see Fig. 2) (Boelens et al. 1988, 1989). Within this approach, theoretical NOE intensities are calculated based on an initial structure that can either be theoretical or based on previous experiments. In a next step, the theoretical intensities are substituted by experimental intensities if available. In this context, the experimental NOE intensities are adjusted by a mixing time specific scaling factor (14)

$$s = \frac{\sum_n a_{ij}(theo)}{\sum_n a_{ij}(\exp)} \tag{14}$$

where a_{ij} is the cross peak intensity between proton i and j of the theoretical and experimental data. The mixed intensity matrix is transformed back into the full relaxation matrix by formula (8). For the extraction of PRE restraints the difference in auto-relaxation rates between diamagnetic NOESY ρ_i^{dia} and paramagnetic NOESY ρ_i^{para} is evaluated. The restraints can then be used for a structure calculation. This procedure can be repeated iteratively with each newly acquired structure.

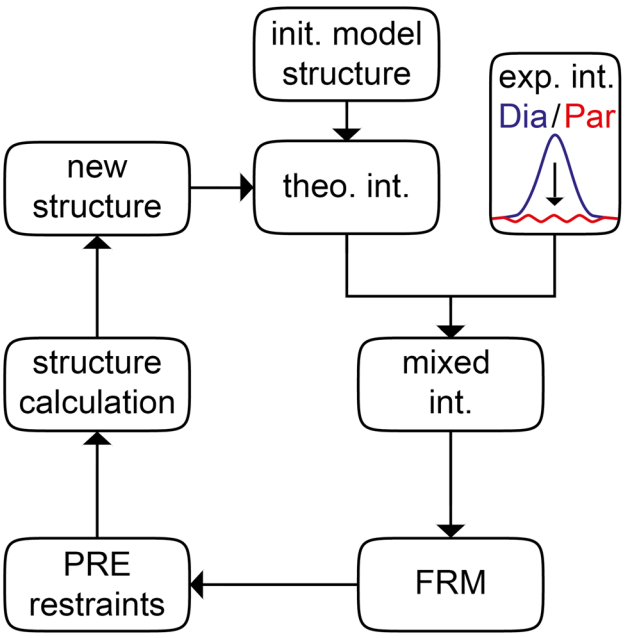

Fig. 2 Schematic of the paramagnetic iterative relaxation matrix approach (P-IRMA) based on IRMA (Boelens et al. 1988, 1989)

Calculations with the FRM

For P-IRMA, two theoretical intensity matrixes need to be constructed—one for the paramagnetic spectra and one for the diamagnetic spectra. Our evaluation script uses the distances of an initial structure bundle (each structure individually) to construct a relaxation matrix [see formula (5)] using formula (1) and (4) for the diamagnetic relaxation matrix and formula (1) and (6) for the paramagnetic relaxation matrix. The multiple relaxation matrixes of each structure of the structure bundle can be averaged to save computing time (which has been done for all structure calculation in this paper). The theoretical intensity matrix can be calculated with the following adaptation of formula (8):

$$A = X_R e^{\Lambda_R \tau_m} X_R^{-1} \tag{15}$$

where X_R contains the eigen vectors of matrix **R** and Λ_R the eigen values of matrix **R**. The intensity matrix **A**(0) from formula (8) was set to the identity matrix to normalize the diagonal peaks to one. After replacing theoretical cross peak intensities with experimental cross peak intensities, whenever possible. The following formula can be used to calculate the FRM.

$$R = \tau_m X_A \ln\left(\Lambda_A\right) X_A^{-1} \tag{16}$$

where X_A contains the eigen vectors of matrix **A** and Λ_A the eigen values of matrix **A**. The PRE rate can be calculated by subtracting each diagonal element of the diamagnetic FRM from the respective diagonal element from the paramagnetic

FRM. The paramagnetic relaxation rate can be back calculated using formula (7) considering the respective correlation times in the spectral density function to determine the PRE restraints. For the construction of the FRM we use formula (2) and (7) with the respective spectral density function to take into account the different correlation times for the electron and the protons. To identify the diamagnetic and paramagnetic components for the back calculation of the distances from the auto relaxation rates we determine the difference of the diagonal elements of the FRM. The PRE distance can be back calculated using a rearranged version of formula (7) using e.g. a correlation time of 2.3 ns for 3 J and a correlation time of 0.5 ns for the 7 J term.

Structure calculation and Implementation

The structure calculation was conducted by CNS 1.1 (Brünger et al. 1998) with an adapted ARIA 1.2 (Linge et al. 2001) implementation, which includes a force field for nucleic acids, OPLS charges and non-binding parameters (Nozinovic et al. 2010). The topology parameters for the modifications 5TPA-U7, 2′TU11 and Çm13 were generated by hand and are based on nucleic acid and protein force fields. For the sake of comparability diamagnetic restraints such as chemical shift lists, NOE intensities, H-bond and base planarity restraints were adapted from 2KOC (Nozinovic et al. 2010). The dihedral restraints have been omitted purposely, to test for the capacity of the P-IRMA approach to improve the quality of the structure. Those restraints are referred to as diamagnetic restraints from here on and were used for all structure calculations to be able to assess the influence of our method and excluding influences of the differences in the NOESY spectra of the spin labelled RNA. PRE-restraints from P-IRMA were determined based on NOESY intensity lists of paramagnetic and diamagnetic spectra respective spin labelled RNAs. The determined restraints were classified in unspecific (below 13 Å or above 20 Å) or specific restraints and were used as ambiguous restraints with an error margin of 3 Å. Specific restraints entered the structure calculation with the determined value (e.g. 17.3 Å), whereas unspecific restraints were only considered as below 13 Å or above 20 Å. Typical distance limits of the PRE effect of nitroxide radicals in literature range on the lower boundary from 12 to 15 Å and on the upper boundary from 20 to 23 Å (Battiste and Wagner 2000; Dedmon et al. 2005; Schnorr et al. 2017). We chose our limits according to the literature. All structure calculations have been conducted 10 times with different initial velocities in order to estimate the error for each structure calculation with otherwise identical parameters.

Between each structure calculation cycle, the best 10 structures were used for the full relaxation matrix (FRM) evaluation. The evaluation script was written in python 2.7 using the libraries NumPy (Walt et al. 2011) and PyMOL (The PyMOL Molecular Graphics System, Version 1.1r2 Schrödinger, LLC) and can be found in the Supporting Information. For the sake of stability and speed of the calculations, the following approximations have been made: The maximal theoretical distance, for which NOE relaxation rates were calculated, was set to 20 Å. Each side of the diagonal (experimental peaks) was evaluated separately, i.e. each crosspeak was inserted symmetrically into the intensity matrix. This means that each side of the diagonal was treated as a separate input. Differences by many orders of magnitudes in the relaxation rate in the full relaxation matrix during the matrix transformation led to instabilities. For the sake of stability the paramagnetic relaxation rate (cf. (7)) was limited to 1000 Hz, correlating for our systens to a distance less than 5 Å. If negative eigenvalues occurred in the transformation of the matrix and those eigenvalues were very small, the absolute value has been used for the matrix transformation. Additionally, very small values in the constructed relaxation matrix ($<9.9E-11$) were set to zero.

Pseudo-experimental data

We deployed our full relaxation matrix approach to calculate intensities to create pseudo experimental data for a given structure. This allowed us to define expected distance restraints and therefore assess the quality of the determined restraints. The full relaxation matrix approach returns a complete intensity matrix, in which crosspeak intensities are indicated as percentage of diagonal peak intensity transferred. To obtain a NOE intensity list similar to experimental sources the full intensity matrix was sorted by the following criteria: cross peak intensities correlating to at least one exchanging partner were removed (as they wouldn't be visible in the experimental D_2O samples), a lower threshold of 0.25% transferred intensity was defined, randomized signal-to-noise, correlating to 0.05% intensity transferred, was added and the cross peak values were multiplied by 10^7.

Results

Analysis of the constructs

Chemical modification of target structures can disturb their three-dimensional structure. Therefore, the location of the paramagnetic group must be carefully planned. In order to validate potential spin label positions, the spin labels have been modelled into the solution structure of the 14-mer RNA to check for collisions of the modification with the RNA. We used this strategy to assess possible positions for the Çm label. In doing so the 2. and 8. base position was ruled out. Similarly the loop positions of for the 2′TU label were

excluded due to the 2′OH positioning in the loop. Therefore the 5TPA-U label was placed in the loop and the other two spin labels were placed in the stem region. Another considered aspect is the spin label flexibility and its impact on the structure calculation. Not only does the flexible spin label add further experimental uncertainty to the distant restraints, but the flexible spin label also needs to be localized, leading to looser structure bundles. Based on these results and with spin label flexibility as an influential parameter for structure calculation in mind, the three spin labels in their current position have been chosen and synthesised.

The impact of the paramagnetic modification on the structure itself must be experimentally assessed. As the chemical shift of a spin is sensitive to its three-dimensional environment, the chemical shift is a sensitive probe for such analyses. The chemical shift changes induced by the different spin-labels in their diamagnetic form used in this work are depicted in Fig. 3. Except in close proximity to the modified nucleobase, the changes in chemical shift for the 5TPA-U spin-label are minor. We therefore assume that the overall three-dimensional structure of the RNA is not disturbed here. In contrast, the constructs incorporating the Çm and 2′TU spin-labels exhibit significantly larger chemical shift changes. For the Çm13 construct, these are mainly located in the stem region, with only small chemical shift differences in the loop region, indicating a localised disruption in the stem region, induced by the spin-label. The perturbations, however, do not necessarily originate solely from the perturbed structure, as the spin label is an extended aromatic system. Theoretical investigations of a small model systems revealed that aromatic systems can influence non-covalently bound proton chemical shifts in close proximity (4.5 Å) (Martin et al. 2008), concluding that the impact of the modified aromatic system on the chemical shift will be greatest in the adjacent base pairs. Therefore, CSPs of basepairs close to the tetraloop can mostly be attributed to perturbances in the structure. For the 2′TU11 construct, on the other hand, the spin-label induced chemical shift changes both in the loop and stem region, suggesting an overall perturbed structure compared to the spin unlabelled 14-mer. These results, however, are not generalizable to the spin label itself, but rather reflect the perturbances of the structure from the specific construct with that certain spin label positioning. This can be illustrated for the Çm13 construct as the same spin label in a different nucleotide sequence exhibited no major chemical shift changes (Schnorr et al. 2017).

Major chemical shift changes, as evidenced for the Çm13 and 2′TU11 constructs, require that long-range distance information obtained from those constructs should not be used for structure calculations as it is uncertain how closely the spin-labelled constructs resemble the unmodified RNA. For the development of our method, however, those two constructs represent very valuable model systems to provide negative controls for our methodological approach. Thus, they are used in the following to analyse how our developed approach copes with experimental data originating from disturbed structures.

Spin label flexibility

The internal motion of the spin label has a large influence on the determination of PRE distances. Not only does the spin label motion introduce a spatial uncertainty to distance restraints, but it also effects the relaxation rate itself (cf. (3) in "Materials and Methods"). The experimentally determined correlation time of the spin labelled site containing

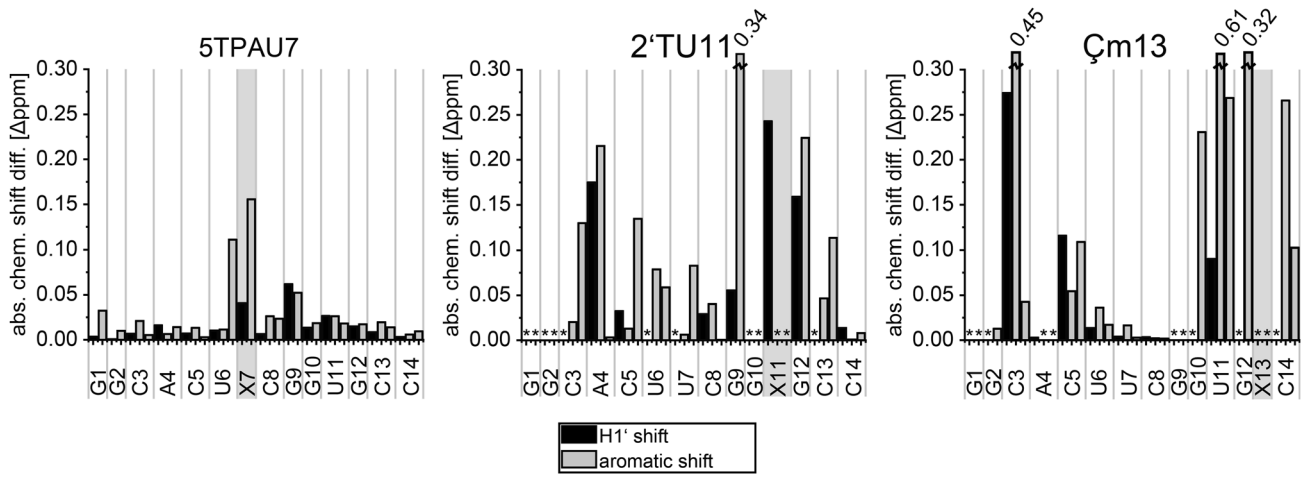

Fig. 3 Proton chemical shift differences between unmodified 14-mer and spin-labelled 14-mer constructs (5TPA-U7, 2T'U11 and Çm13) extracted from NOESY assignments for H1′ (black bars) and the aromatic protons (grey bars). The asterisks mark protons that could not be assigned. The spin-labelled bases are highlighted in grey

the electron allows for important insight into the spin label motion. Table 1 shows the correlation times for the individual constructs determined by EPR line-width analysis with *easyspin* (Stoll and Schweiger 2006) by fitting simulated EPR spectra to the experimental data (see SI, Table 1). The short isotropic τ_c of 0.5 ns for the 5TPA-U7 and 2′TU11 constructs highlight the corresponding spin label flexibility, whereas the spin label in the Çm13 construct is rigid as the correlation time of the electron mostly arises from the rotational correlation time of the RNA itself. The experimental data have also been fitted to an anisotropic model (see SI, Table 2) with no improvements for the flexible spin labels 5TPA-U7 and 2′TU11. However, the RMSD between theoretical curve and experimental data improved significantly for the spin label Çm13, exhibiting a correlation time of 361.4 ns in one of the axis, which exceeds the isotropic movement of the molecule by two orders of magnitude. This renders the internal movement of the Çm13 spin label insignificant for relaxation.

The effect of the correlation time τ_c on the NOE build-up curves has been simulated for different electron proton distances and is shown in Fig. 4. It illustrates that although the PRE effect is an auto relaxation effect, it influence is observable in the cross peak intensities. The signal reduction is distinctive for protons in close proximity to the unpaired electron for all correlation times. The curves also illustrate the correlation time dependence of the PRE: smaller correlation times induce more pronounced signal attenuation than larger ones. With increasing distance between the electron and proton, the signal decrease becomes less dominant. This is especially valid for short mixing times, which are preferably used for NOE distance determination to minimise the effect of spin diffusion. For distance determination based on PRE, however, the use of higher mixing times leads to the most pronounced differences in signal intensities, yet requires accurate description of spin diffusion. Thus, while high mixing times theoretically yield the maximum difference between diamagnetic and paramagnetic intensities, other factors such as signal overlap and accuracy of the determined distances also need to be considered from a practical point of view.

Table 1 Correlation times of the electron determined by EPR line-width analysis of 5TPA-U7, 2′TU11 and Çm13 at room temperature (For plots of the fits see SI) and rotational correlation time of the unmodified UUCG tetraloop 14-mer at room temperature as orientation determined from NMR (Duchardt and Schwalbe 2005)

Construct	*Isotropic* τ_c (EPR)	τ_c (NMR)
Unmodified		2.3 ns
5TPA-U7	0.5 ns	
2′TU11	0.5 ns	
Çm13	1.9 ns	

The mixing time dependence of the restraint accuracy has been evaluated for 5TPA-U7 for two different structure bundles: (i) a bundle consisting of ten randomized structures used as negative control experiment and (ii) a tight bundle that closely resembles the reference structure (with the additional spin-label). To this end, the restraints determined with the experimental intensities of the 5TPA-U7 RNA after a single iteration of the P-IRMA approach were compared to the reference distances. This happened under the assumption (based on the CSP analysis) that the 5TPA modification did not perturb the structure of the molecule. Figure 5a shows the mean absolute deviation (MAD) obtained at different mixing times. In line with expectation, the MAD of structure bundle (i) is significantly higher than that of (ii). Structure bundle (ii) exhibits marginal MADs for all mixing times investigated. The (slightly)

Table 2 Influence of the spin-label and P-IRMA on (a) precision (ensemble RMSD) and (b) accuracy (alignment RMSD towards 2KOC) of the structure calculations

	Unmod. 14-mer	5TPA-U7	5TPA-U7 + P-IRMA	2′TU11	2′TU11 + P-IRMA	Çm13	Çm13 + P-IRMA
(a) Precision							
Overall	1.78 ± 0.07	*2.2 ± 0.1*	1.72 ± 0.06	*2.2 ± 0.3*	**1.45 ± 0.07**	*2.8 ± 0.5*	**1.6 ± 0.2**
Loop	1.5 ± 0.1	*2.5 ± 0.2*	*1.86 ± 0.06*	1.46 ± 0.06	**1.22 ± 0.07**	1.6 ± 0.2	1.6 ± 0.3
Stem	1.79 ± 0.08	1.8 ± 0.2	**1.56 ± 0.07**	*2.3 ± 0.3*	**1.48 ± 0.08**	*2.9 ± 0.6*	**1.5 ± 0.1**
(b) Accuracy							
Overall	1.00 ± 0.09	**0.88 ± 0.05**	**0.86 ± 0.05**	*1.2 ± 0.2*	*1.3 ± 0.2*	1.0 ± 0.1	*1.2 ± 0.1*
Loop	0.61 ± 0.05	0.58 ± 0.04	**0.52 ± 0.02**	*0.71 ± 0.06*	*0.71 ± 0.05*	0.61 ± 0.05	*0.68 ± 0.05*
Stem	0.88 ± 0.08	0.85 ± 0.04	**0.80 ± 0.05**	*1.1 ± 0.1*	*1.1 ± 0.2*	0.9 ± 0.1	*1.08 ± 0.08*

All structure calculations were performed in sets of ten to estimate the margin of error corresponding to a confidence interval of 95%. The table is colour-coded to indicate statistically significant improvements (bold values) and significant worsening (italic values) of the structure bundles of spin-labelled constructs in comparison to the unmodified 14-mer. The stated RMSDs correspond to the following nucleobases: overall (2–13), loop (6–9) and stem (2–6 and 9–13)

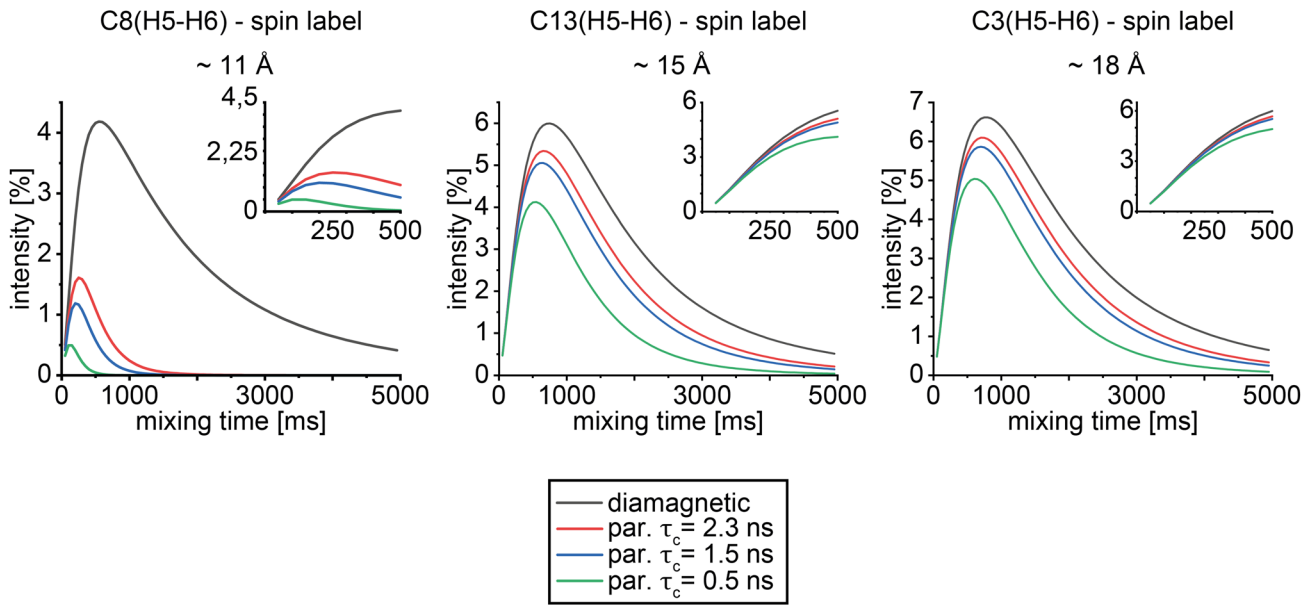

Fig. 4 Theoretical build-up curves of selected peaks (with different distances to the spin label) calculated for correlation times $\tau_c = 0.5$ ns, 1.5 ns and 2.3 ns and a diamagnetic reference, using a full relaxation matrix approach based on a model structure for 5TPA-U7 with close resemblance to 2KOC (structure can be found in SI)

increased MAD at longer mixing times can be rationalised by the growing impact of the PRE effect, which is also accompanied by the stronger effect of experimental noise on distance restraints obtained. For structure bundle (i), on the other hand, the high MAD originates from a large difference between experimental and theoretical intensities. The inaccurate initial structure bundle introduces an error significantly larger than the experimental noise, thus leading to orthogonality of mixing time and MAD. At this point it is important to point out, that P-IRMA in contrast to IRMA is sensitive to global structure changes. This can be explained by the longer range of the PRE Effect in comparison to the interatomic NOE.

Another important feature of Fig. 5a is the increasing error bar of structure bundle (ii) with increasing mixing times. This means, that higher mixing times result in higher variations of the determined restraints from the expected value. This is also illustrated by the comparison between Fig. 5b and c. Furthermore, restraints below 8 Å deviate from the expected diagonal line. This artefact can most likely be ascribed to the approximation to limit the maximal relaxation rate in the construction of the FRM to 1000 Hz. However, this is inconsequential to the structure calculations as distances below 13 Å are classified as unspecific restraints.

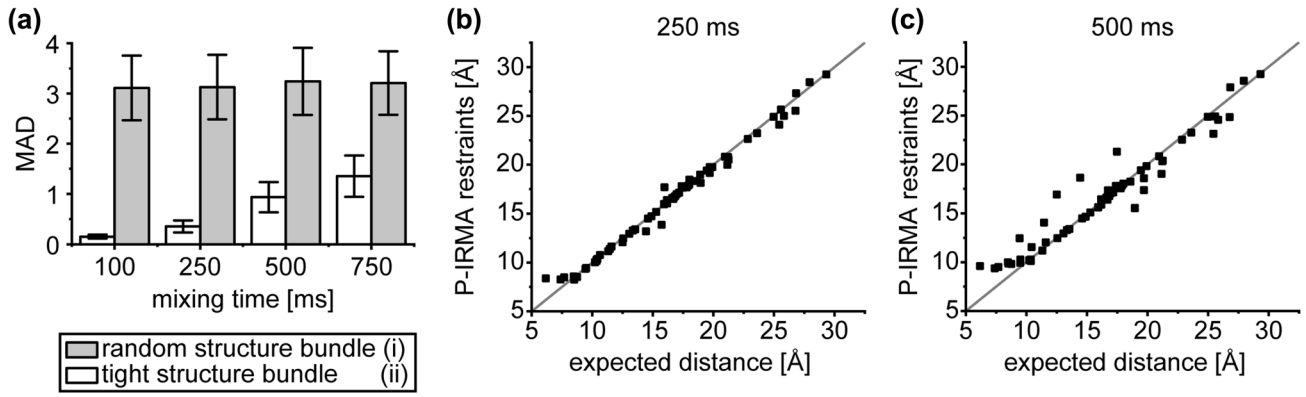

Fig. 5 **a** MAD of PRE restraints calculated from 100 to 750 ms using the FRM approach based on a randomized structure bundle and a tight structure bundle (closest to 2KOC). Plot of the expected distance against the determined P-IRMA restraints at different mixing times, **b** 250 ms and **c** 500 ms. Plots of the other mixing times can be found in the SI (Fig. 3)

Further, the number of assignable peaks for our system substantially increases from mixing times of 100–250 ms and the respective MADs are essentially identical within error bars, so that we use mixing times in the order of 250 ms for all experiments reported in the following. No additional peak information is obtained at mixing times of 500 ms or higher.

Full relaxation matrix (FRM) approach

The decrease of NOESY intensities upon introduction of a spin-label shown in Fig. 6 qualitatively illustrates the distance dependence of the PRE effect. Generally, the latter is evaluated by a relaxation delay-dependent signal decrease (Iwahara et al. 2007). This approach, however, is not straightforward for PRE data obtained from NOESY spectra, because every peak contains information on three different distances, two of which correspond to proton-electron distances in addition to the common proton–proton NOE distance. Simple fitting of the exponentially decaying signal (paramagnetic intensity subtracted from the diamagnetic Intensity) returns only one average proton-electron distance: By comparing the experimental data with a simplified three spin system (containing both involved nuclei and the electron) we were able to estimate the corresponding distance. However, distances estimated in this way are generally too short due to spin diffusion (Kalk and Berendsen 1976).

Therefore, we employed a FRM approach to estimate the PRE distance restraints, in which theoretical intensities are calculated from an initial model structure. In addition to including spin diffusion into the evaluation of the restraints (Boelens et al. 1988), the distance-dependent signal intensity decrease of the whole spectrum was analysed simultaneously, so that every cross peak of each proton contributes to the PRE restraints for that proton. For example, the signal decreases of the cross peaks U6H5-H6, U6H3′-H6 and U6H2′-H6 all contribute to the PRE distance restraint for the U6H6-electron.

For the extraction of meaningful experimental restraints, the influence of the initial—and possibly incorrect—structure must be smaller than the influence of the experimental data. As two of the three spin labels investigated are known to introduce a change to the three-dimensional structure of the constructs, the assessment of restraint quality poses a challenge. In a first step, we therefore calculated pseudo-experimental data from a known three-dimensional model (see the "Materials and Methods"section for further details), allowing for a direct comparison of the acquired restraints and the corresponding distances in the underlying model. In a second step, these pseudo-experimental data were used in the calculation of PRE restraints starting from a randomized structure bundle. The quality of the restraints obtained, summarised by nucleobase, is depicted in Fig. 7.

Even though the structure bundle used for calculation of the theoretical intensities is distinctively wrong, most restraints deviate less than 3 Å from the expected value, which is the range of typical errors assumed for structure calculations with PRE restraints (Battiste and Wagner 2000; Volkov et al. 2006). The larger deviations can be attributed to the influence of the model structure bundle, hence illustrating the need for an iterative approach to obtain a better structure basis.

As the structure bundle converges, the difference between the model structure bundle used and the actual structure described by the experimental data decreases (Fig. 8, underlying model is the structure bundle of the first iteration of a structure calculation without PRE restraints). This loosely formed hairpin structure resembles the reference structure significantly better than the randomized bundle, so that the quality of the restraints naturally increases. The restraints for the 2′TU11 and Çm13 constructs in average deviate less than 1 Å from the expected values. The higher deviation for the restraints of the 5TPA-U7 construct can be explained by the high flexibility of the loop region the spin-label is attached to. The fluctuation of the unrestrainted spin label position in the model of up to 8 Å is reflected in the higher deviation

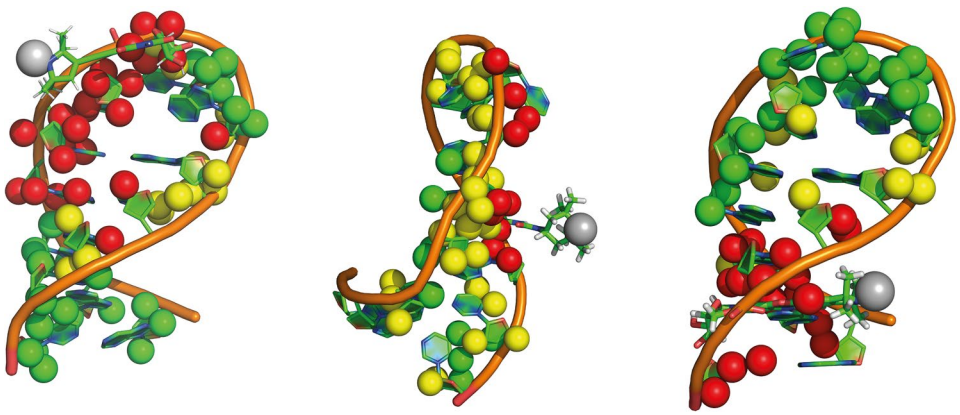

Fig. 6 Qualitative analysis of NOESY intensities. Unpaired electron labelled in grey, detected protons coloured depending on the average signal intensity decrease induced by the paramagnetic species. Red: average signal decrease of more than 66%; yellow: signal decrease between 33 and 66%; green: signal decrease of less than 33%

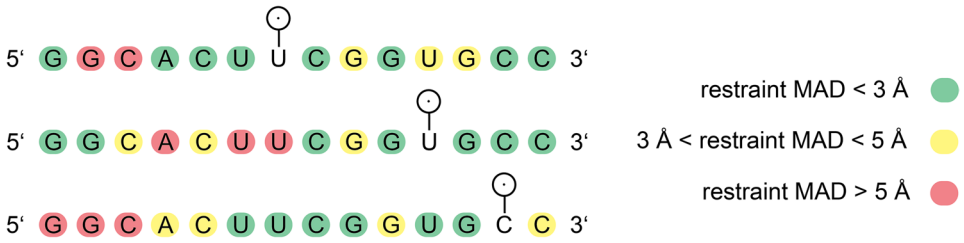

Fig. 7 MAD of distance restraints for 5TPA-U7 (top), 2′TU11 (middle) and Çm13 (bottom) summarised by nucleo base compared to reference structure, obtained from FRM approach. Restraints were calculated from a randomized structure bundle using pseudo-experimental data with a defined reference structure. Total MAD 5TPA-U7: 2.1 Å, 2′TU11: 2.7 Å and Çm13: 3.7 Å

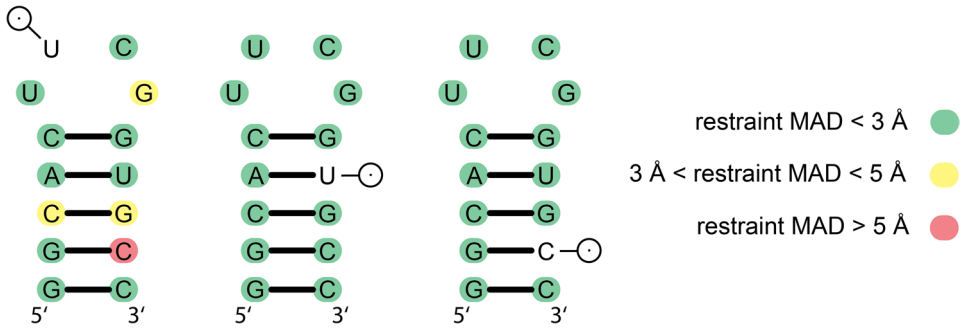

Fig. 8 MAD of distance restraints for 5TPA-U7 (left), 2′TU11 (middle) and Çm13 (right) summarised by nucleobase compared to reference structure, obtained, from FRM approach. Restraints were calculated from a hairpin structure bundle using pseudo-experimental data with a defined reference structure. Total MAD 5TPA-U7: 2.0 Å, 2′TU11: 0.6 Å and Çm13: 0.4 Å

of the calculated restraints, which emphasises the necessity for an iterative approach.

In summary, evaluation of our approach using a single P-IRMA iteration and pseudo-experimental data showed that most of the calculated restraints are within an error typical for PRE restraints if a good starting structure is used. Yet, as in most cases the starting structure deviates significantly from the actual structure, an iterative P-IRMA approach is generally needed to resolve the three-dimensional structure of any given biomolecule.

P-IRMA

As the restraints for the unmodified 14-mer tetraloop already describe the structure well, we excluded torsion angle restraints in order to observe the effect of PRE restraints on the structure calculation. To assess the effect of supplementary paramagnetic restraints and the spin-label introduced additional degrees of freedom on the structure calculation, three sets of different structure calculations were conducted for each construct. The first structure calculation was conducted with an unmodified 14-mer RNA and serves as reference structure calculation. The spin-label modification was added in the second (for figure see SI) set of structure calculations and contains the exact same restraints as the first set with the difference that the input RNA contains the respective spin labels. The strategy behind this is that the difference between the first two sets of structure calculations should illustrate the impact of the spin label addition on the structure calculation. The third set of structure calculations were carried out as the second set with the additional use of P-IRMA. The three sets of generated structure bundles were evaluated with respect to precision (ensemble RMSD) and accuracy (alignment RMSD to the already published 14-mer reference structure 2KOC) (Table 2).

Figure 9 displays exemplary structure bundles with the use of P-IRMA restraints. Introduction of the spin label in 5TPA-U7 without further restraints loosens the structure bundle, especially in the modified (loop) region (for figure see SI). Employment of the P-IRMA procedure leads to a higher RMSD in the loop region compared to the unmodified system. However, overall precision is increased as the ensemble RMSD decreases, as is the alignment of the structure bundle to the reference structure 2KOC, an adequate indicator for the method accuracy, which significantly improves for the 5TPA-U7 construct upon employment of the P-IRMA approach.

Similar observations regarding precision can be made for the 2′TU11 and Çm13 constructs. Incorporation of the spin labels into the structures introduces more degrees of

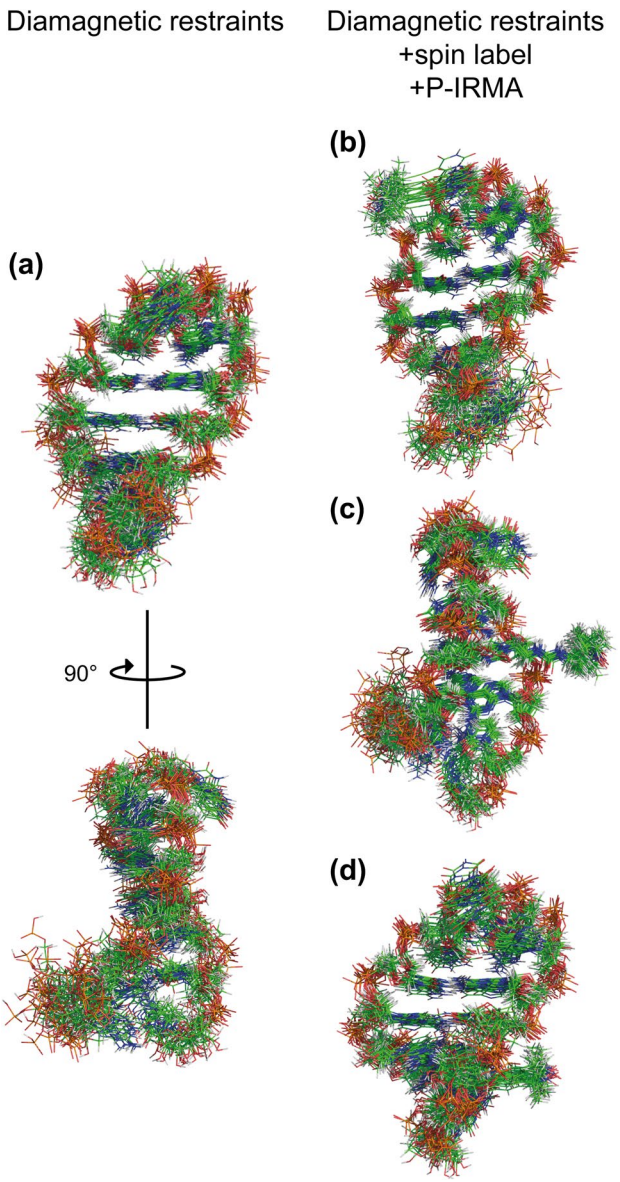

Fig. 9 Effect of the spin-label addition and P-IRMA on the structure calculation. **a** Reference structure calculation of the unmodified 14-mer construct, calculated with diamagnetic restraints only. **b** 5TPA-U7, **c** 2′TU11 and **d** Çm13 structure bundle determined utilizing diamagnetic restraints with the P-IRMA protocol

freedom, which lead to a loosening of the RMSD localized in the stem region, where both spin-labels are located. In both cases, use of our P-IRMA procedure can compensate for the additional degrees of freedom, returning a tigher structure bundle than the structure calculation of the unmodified 14-mer. The accuracy of the structure bundles for these two constructs, however, exhibit opposite trends compared to the 5TPA-U7 construct: structure bundles for 2′TU11 and Çm13 deviate stronger from 2KOC upon employment of the P-IRMA procedure. This finding fits well our experimental chemical shift analysis results, which suggested a significant structural perturbance.

Furthermore, the analysis was also performed with pseudo experimental data. The expected result of this set of structure calculations was that the accuracy and precision structure bundle increases. And indeed the 5TPA-U7 and Çm13 RNA structure bundles showed improved precision and accuracy values. Implicating that the perturbed structure of the Çm13 in Fig. 9d indeed originates from the experimental intensities. However, this effect cannot be observed for pseudoexperimental data of 2′TU11 RNA. A possible explanation might be that the additional PRE restraints cannot be fully exploited due to the spin label flexibility (Table 3).

The nature of the perturbances have been evaluated by a base pair wise determination of the accuracy and the precision (for table see SI). Where the precision (ensemble RMSD) is analogous to the stem wide analysis, the accuracy (alignment RMSD towards 2KOC) features some deviations. The local perturbances in the structure of 5TPA-U7 and 2′TU11 are in line with the global findings. However, the local disturbance for the Çm13 spin label are minimal in contrast to the global analysis. The minimal local perturbations in the context of significant global perturbations for the Çm13 construct can be reasoned with the positioning of the spin label, as the second last position in the stem is an unfavourable position for the spin label and it seems to lead to a distortion of the overall structure without interfering with the individual base pairing.

In summary, employment of the P-IRMA procedure leads to a decrease of the overall RMSD, which can be locally offset by the spin label. More importantly, however, is the coherence between the resulting structure bundles and our experimental chemical shift analysis. Constructs exhibiting strong chemical shift changes return perturbed structures, whereas the 5TPA-U7 construct, which shows only minute chemical shift changes, is accurately described with reference to 2KOC.

Conclusion

In this work, we presented an approach for the extraction and evaluation of PRE restraints for structure calculations from 2D ^{1}H-^{1}H-NOESY experiments, motivated by extensive efforts associated with isotope- and spin-labelling of RNA molecules. This approach yields PRE restraints after each iteration of a structure calculation, evaluating a full relaxation matrix computed from experimental intensities and the current structure bundle.

As the correlation time of the electron and hence the spin-label flexibility has an effect on the strength of the PRE effect, we validated our approach on three 14-mer RNA

Table 3 Influence of the spin-label and P-IRMA with pseudo experimental data on (a) precision (ensemble RMSD) and (b) accuracy (alignment RMSD towards 2KOC) of the structure calculations

	Unmod. 14-mer	5TPA-U7	5TPA-U7 + P-IRMA	2′TU11	2′TU11 + P-IRMA	Çm13	Çm13 + P-IRMA
(a) Precision							
Overall	1.78 ± 0.07	*2.2 ± 0.1*	1.76 ± 0.06	*2.2 ± 0.3*	**1.57 ± 0.06**	*2.8 ± 0.5*	1.7 ± 0.3
Loop	1.5 ± 0.1	*2.5 ± 0.2*	*1.9 ± 0.1*	1.46 ± 0.06	**1.26 ± 0.08**	1.6 ± 0.2	1.42 ± 0.09
Stem	1.79 ± 0.08	1.8 ± 0.2	**1.59 ± 0.05**	*2.3 ± 0.3*	**1.6 ± 0.07**	*2.9 ± 0.6*	1.7 ± 0.3
(b) Accuracy							
Overall	1.00 ± 0.09	**0.88 ± 0.05**	**0.85 ± 0.06**	*1.2 ± 0.2*	*1.12 ± 0.06*	1.0 ± 0.1	0.95 ± 0.06
Loop	0.61 ± 0.05	0.58 ± 0.04	**0.53 ± 0.02**	*0.71 ± 0.06*	0.67 ± 0.05	0.61 ± 0.05	0.59 ± 0.04
Stem	0.88 ± 0.08	0.85 ± 0.04	**0.80 ± 0.06**	*1.1 ± 0.1*	*1.0 ± 0.1*	0.9 ± 0.1	0.83 ± 0.06

All structure calculations were performed in sets of ten to estimate the margin of error corresponding to a confidence interval of 95%. The table is colour-coded to indicate statistically significant improvements (bold values) and significant worsening (italic values) of the structure bundles of spin-labelled constructs in comparison to the unmodified 14-mer. The stated RMSDs correspond to the following nucleobases: overall (2–13), loop (6–9) and stem (2–6 and 9–13)

constructs with spin-labels of varying flexibility. The evaluation of theoretical build-up curves in a correlation-time dependent manner confirmed that smaller correlation times exhibit stronger PRE effects. Additionally, the build-up curves revealed that low mixing times, typical for the evaluation of NOE intensities, are unsuitable for PRE distance determination as the impact of the paramagnetic effect is minimal. Further analysis of the dependency of the distance restraint quality on the mixing time revealed an increase of MAD with higher mixing times. Furthermore, the number of assignable crosspeaks plateaus at 250 ms for the present system, so that we suggest using mixing times around 250 ms.

We examined the impact of the theoretical model structure on the determined restraints. Despite the influence of a randomized structure bundle, the worst starting point for our iterative approach on the determined restraints, MADs were within or close to an error range typical for PRE restraints. A better initial structure significantly decreased the number of restraints that were erroneous by more than 3 Å, illustrating the improvements of PRE restraints upon use of an iterative procedure during the structure calculation.

As chemical modification of the RNA can always perturb its structure, we reassessed the chemical shifts of the modified constructs. Two of the constructs featured significant chemical shift changes, indicating a perturbance of the structure. Those two constructs (2′TU11 and Çm13) served as negative control for our evaluation of the method, revealing that additional PRE restraints decrease the RMSD of the structure bundle. Additionally, assessment of the method's accuracy by determination of the alignment RMSD towards the 2KOC reference structure shows a good correlation between RMSD and chemical shift analysis. Alignment of the 5TPA-U7 structure bundle towards the reference structure improved with supplementary P-IRMA restraints, whereas the other two constructs, in line with expectations, deviated from the reference structure upon use of P-IRMA. An examination of local perturbances revealed a difference between the constructs 2′TU11 and Çm13. Where the 2′TU spin label caused global and local perturbations, the Çm spin label showed mostly a global distortion. It is likely that the distortion caused by Çm is a result of the positioning the spin label close to the end of the helix and that this distortion could be compensated by elongating the stem. It should be noted that our results are not generalizable for the spin labels that were investigated here, as many factors such as structure of the target RNA and spin label position need to be assessed for each individual RNA.

P-IRMA has been developed as a method for structural refinement and the structures that have been perturbed by the spin label served as important negative controls from a method development stand point. The approach for the assessment of the structural impact of a spin labels can be generally transferred to any NMR sample (independently of isotope labelling). The full relaxation matrix approach can also be facilitated beyond structural refinement when the system under investigation is already structurally well-defined with no perturbances by the spin label. The model free approach (see formula 9–13) can be used to incorporate spin label motion into the construction of the FRM to calculate NOE intensities that contain previously simulated spin label motion. The comparison of these theoretical NOE intensities with experimental NOE intensities could be used to evaluate the impact of spin label motion.

To conclude, the P-IRMA approach based on 2D ^{1}H–^{1}H-NOESY intensities is a useful tool for structure refinement of spin-labelled RNA that renders costly isotope-labelling dispensable. Taking advantage of the PRE effect, it provides access to long-range distance information and appears to be generalizable for the three-dimensional structure elucidation of larger nucleic acids.

Acknowledgements E.C.C. gratefully acknowledges a MainCampus scholarship provided by the Stiftung Polytechnische Gesellschaft (Frankfurt). We would like to thank E. Stirnal, M. Gränz and E. Jaumann for help with experiments. The work was supported by DFG through CRC902 and by the state of Hesse through institutional funding to BMRZ.

References

Azarkh M, Singh V, Okle O, Seemann IT, Dietrich DR, Hartig JS, Drescher M (2013) Site-directed spin-labeling of nucleotides and the use of in-cell EPR to determine long-range distances in a biologically relevant environment. Nat Protoc 8:131–147

Battiste JL, Wagner G (2000) Utilization of site-directed spin labeling and high-resolution heteronuclear nuclear magnetic resonance for global fold determination of large proteins with limited nuclear overhauser effect data†. Biochemistry 39:5355–5365

Beswick V, Guerois R, Cordier-Ochsenbein F, Coïc Y-M, Huynh-Dinh T, Tostain J, Noël J-P, Sanson A, Neumann J-M (1998) Dodecylphosphocholine micelles as a membrane-like environment: new results from NMR relaxation and paramagnetic relaxation enhancement analysis. Eur Biophys J 28:48–58

Boelens R, Koning TMG, Kaptein R (1988) Determination of biomolecular structures from proton-proton NOE's using a relaxation matrix approach. J Mol Struct 173:299–311

Boelens R, Koning TMG, van der Marel GA, van Boom JH, Kaptein R (1989) Iterative procedure for structure determination from proton-proton NOEs using a full relaxation matrix approach. Application to a DNA octamer. J Magn Reson 82:290–308

Brueschweiler R, Roux B, Blackledge M, Griesinger C, Karplus M, Ernst RR (1992) Influence of rapid intramolecular motion on NMR cross-relaxation rates. A molecular dynamics study of antamanide in solution. J Am Chem Soc 114:2289–2302

Brünger AT, Adams PD, Clore GM, DeLano WL, Gros P, Grosse-Kunstleve RW, Jiang JS, Kuszewski J, Nilges M, Pannu NS et al (1998) Crystallography & NMR system: a new software suite for macromolecular structure determination. Acta Crystallogr D 54:905–921

Büttner L, Seikowski J, Wawrzyniak K, Ochmann A, Höbartner C (2013) Synthesis of spin-labeled riboswitch RNAs using convertible nucleosides and DNA-catalyzed RNA ligation. Bioorg Med Chem 21:6171–6180

Dedmon MM, Lindorff-Larsen K, Christodoulou J, Vendruscolo M, Dobson CM (2005) Mapping long-range interactions in α-synuclein using spin-label NMR and ensemble molecular dynamics simulations. J Am Chem Soc 127:476–477

Duchardt E, Schwalbe H (2005) Residue specific ribose and nucleobase dynamics of the cUUCGg RNA tetraloop motif by MNMR 13C relaxation. J Biomol NMR 32:295–308

Edwards TE, Sigurdsson ST (2007) Site-specific incorporation of nitroxide spin-labels into 2′-positions of nucleic acids. Nat Protoc 2:1954–1962

Fürtig B, Richter C, Bermel W, Schwalbe H (2004) New NMR experiments for RNA nucleobase resonance assignment and chemical shift analysis of an RNA UUCG tetraloop. J Biomol NMR 28:69–79

Grünewald C, Kwon T, Piton N, Förster U, Wachtveitl J, Engels JW (2008) RNA as scaffold for pyrene excited complexes. Bioorg Med Chem 16:19–26

Helmling C, Bessi I, Wacker A, Schnorr KA, Jonker HRA, Richter C, Wagner D, Kreibich M, Schwalbe H (2014) Noncovalent spin labeling of riboswitch rnas to obtain long-range structural NMR restraints. ACS Chem Biol 9:1330–1339

Höbartner C, Sicoli G, Wachowius F, Gophane DB, Sigurdsson STh (2012) Synthesis and characterization of RNA containing a rigid and nonperturbing cytidine-derived spin label. J Org Chem 77:7749–7754

Iwahara J, Tang C, Marius Clore G (2007) Practical aspects of 1H transverse paramagnetic relaxation enhancement measurements on macromolecules. J Magn Reson 184:185–195

Kalk A, Berendsen HJC (1976) Proton magnetic relaxation and spin diffusion in proteins. J Magn Reson 1969(24):343–366

Kellner R, Mangels C, Schweimer K, Prasch SJ, Weiglmeier PR, Rösch P, Schwarzinger S (2009) SEMPRE: spectral editing mediated by paramagnetic relaxation enhancement. J Am Chem Soc 131:18016–18017

Linge JP, O'Donoghue SI, Nilges M (2001) Automated assignment of ambiguous nuclear overhauser effects with ARIA. Methods in Enzymology 339:71–90

Lipari G, Szabo A (1982) Model-free approach to the interpretation of nuclear magnetic resonance relaxation in macromolecules. 1. Theory and range of validity. J Am Chem Soc 104:4546–4559

Mackereth CD, Madl T, Bonnal S, Simon B, Zanier K, Gasch A, Rybin V, Valcárcel J, Sattler M (2011) Multi-domain conformational selection underlies pre-mRNA splicing regulation by U2AF. Nature 475:408–411

Macosko JC, Pio MS, Tinoco I, Shin Y-K (1999) A novel 5′ displacement spin-labeling technique for electron paramagnetic resonance spectroscopy of RNA. RNA 5:1158–1166

Martin NH, Floyd RM, Woodcock HL, Huffman S, Lee C-K (2008) Computation of through-space NMR shielding effects in aromatic ring π-stacked complexes. J Mol Graph Model 26:1125–1130

Nozinovic S, Fürtig B, Jonker HRA, Richter C, Schwalbe H (2010) High-resolution NMR structure of an RNA model system: the 14-mer cUUCGg tetraloop hairpin RNA. Nucleic Acids Res 38:683–694

Ramos A, Varani G (1998) A new method to detect long-range protein–RNA contacts: nMR detection of electron–proton relaxation induced by nitroxide spin-labeled RNA. J Am Chem Soc 120:10992–10993

Schiemann O, Piton N, Plackmeyer J, Bode BE, Prisner TF, Engels JW (2007) Spin labeling of oligonucleotides with the nitroxide TPA and use of PELDOR, a pulse EPR method, to measure intramolecular distances. Nat Protoc 2:904–923

Schnorr K, Gophane DB, Helmling C, Cetiner E, Pasemann K, Fürtig B, Wacker A, Qureshi NS, Gränz M, Barthelmes D et al (2017) Impact of spin label rigidity on extent and accuracy of distance information from PRE data. J Biomol NMR 68:53–63

Seven I, Weinrich T, Gränz M, Grünewald C, Brüß S, Krstić I, Prisner TF, Heckel A, Göbel MW (2014) Photolabile protecting groups for nitroxide spin labels. Eur J Org Chem 2014:4037–4043

Solomon I (1955) Relaxation processes in a system of two spins. Phys Rev 99:559–565

Stoll S, Schweiger A (2006) EasySpin, a comprehensive software package for spectral simulation and analysis in EPR. J Magn Reson 178:42–55

Unger SW, Lecomte JTJ, La Mar GN (1985) The utility of the nuclear overhauser effect for peak assignment and structure elucidation in paramagnetic proteins. J Magn Reson 64:521–526

van der Walt S, Colbert SC, Varoquaux G (2011) The numPy array: a structure for efficient numerical computation. Comput Sci Eng 13:22–30

Volkov AN, Worrall JAR, Holtzmann E, Ubbink M (2006) Solution structure and dynamics of the complex between cytochrome

c and cytochrome c peroxidase determined by paramagnetic NMR. Proc Natl Acad Sci 103:18945–18950

Wunderlich CH, Huber RG, Spitzer R, Liedl KR, Kloiber K, Kreutz C (2013) A novel paramagnetic relaxation enhancement tag for nucleic acids: a tool to study structure and dynamics of RNA. ACS Chem Biol 8:2697–2706